Journal of Thermal Analysis and Calorimetry, Vol. 69 (2002) 149–161

SHAPE ANALYSIS OF DSC ICE MELTING ENDOTHERMS
Towards an estimation of the instrumental profile

V. T. Popa[1] *and E. Segal*[2]

[1]Roumanian Academy, 'I. G. Murgulescu' Institute of Physical Chemistry, Splaiul Independentei 202, Bucharest 77208, Roumania
[2]Bucharest University, Department of Physical Chemistry, Bd. Elisabeta 2 - 12, Bucharest 70346, Roumania

Abstract

DSC endotherms of ice melting in hermetically sealed aluminum pans are analyzed by means of fitting functions derived for spectroscopy and chromatography signal processing. Two sets of experiments are performed: 1) variable heating rate, investigated between 1–5 K min^{-1} for a small sample of 0.3 mg, and 2) variable sample mass, for different samples within 2–11 mg. Variations of both broadness and shape of the corresponding endotherms are observed and analyzed.

Heating rate influence is best described by an intermediate form of the Pearson IV function, derived and widely used in statistics and also in chromatography, and found to accurately account for the instrumental profile. Thermal transfer through the outer (calorimeter/pan) and inner (pan/sample) interfaces of hermetical Al pans is suspected as the main contributor to the shape of the observed endotherms. An important threshold in their shape is noticed between heating rates of 1 and 2 K min^{-1}, where peaks plotted in temperature scale change from fronted to tailed. For time scale plotted peaks the same change occurs between 3 and 4 K min^{-1}. Symmetrical spectroscopic functions are not suitable for the correct description of the observed shape effects.

At least in a formal manner, mass influence closely resembles the column overload effects in gas chromatography, where axial diffusion and dispersion take place. The GC derived HVL (Haarhoff–Van der Linde) function offers an excellent fit of endotherms with mass overload. This apparent coincidence is ascribed to an initial partial melting that makes most of the remaining melting process to be controlled by thermal transfer across the liquid interface layer thus formed.

Keywords: asymmetry, heating rate and mass effects, ice melting, peak fitting, shape

Introduction

The signal patterns of differential thermal analysis (DTA) and differential scanning calorimetry (DSC) contain, in many instances, features that resemble and are even given the name of 'peaks'. Not infrequently these components of a DTA or DSC curve either overlap or are distorted by various instrumental factors, in a manner that closely resembles the current situation in other instrumental techniques, such as spectroscopy and chromatography. However, a refined and powerful approach to signal processing such as that devel-

1418–2874/2002/ $ 5.00

Akadémiai Kiadó, Budapest
Kluwer Academic Publishers, Dordrecht

oped, e.g., in spectroscopy, is not available in thermal analysis, with the noteworthy exception of temperature modulated differential scanning calorimetry (TMDSC) [1, 2], where extensive use is made of Fourier analysis [3, 4].

Melting processes are good sources of thermal peaks. Within the thermoporometry method of Brun *et al.* [5], confined ice melting seemed an interesting alternative in the investigation of porous materials, especially in the case of organic membranes [6, 7] the dry structure of which is far from the wet, swollen one, active in ultrafiltration. A detailed critical study of Cuperus *et al.* [8] questioned the suitability of thermoporometry for the characterization of ultrafiltration membranes. One of the main reasons of skepticism was the interference between outer, 'normal' ice, and inner, pore – confined ice and the overlapping of their corresponding thermal signals. In a recent TMDSC study [9], Knopp and Nail found that the standard error in the determination of ice mean heat capacity exhibited an unpredictable trend with the temperature and period of modulation, ascribed to variations in sample geometry within melting – freezing cycles. The kinetics of ice cubes melting in a constant temperature water flow was investigated even more recently by Galwey *et al.* [10], within the temperature range 276.2–303.4 K. Most of the data obeyed well the contracting volume rate equation (derived for solid state reactions), with apparent activation energy close to that of the hydrogen bond in ice, and pointing to the rupture of such bonds as the rate determining step. This description fails for the lowest temperatures of the water flow thus driving the authors to the conclusion that the melting rate is better represented by the interface advance model and controlled by thermal transfer across the boundary liquid layer.

It seems that melting in general, and that of ice in particular, deserves a closer and somewhat fresh look. In DSC, it produces well-defined peaks, the shape and size of which is sensitive to experimental factors such as heating rate and sample mass. The objective of this contribution consists of the shape analysis of ice melting endotherms, with tools borrowed from spectroscopy and chromatography, and a quantitative representation of the influence of the above factors.

Experimental

All melting experiments were performed on a computer – interfaced DuPont 1090 Thermal Analyzer with a 901 DSC base module and pressure DSC cell in static, ambient atmosphere. A stainless steel cooling can, under liquid nitrogen, served for freezing of the water samples. Hermetically sealed aluminum pans were used for both variable heating rate and variable mass runs. As this is the standard (manufacturer recommended) choice when dealing with liquids, the investigation of its possible influence on the shape of the observed thermal effects seems justified. The influence of the heating rate, '*Hr*', was investigated in runs with 1, 2, 3, 4, and 5 K min^{-1} on a 0.3 mg water sample, while samples with masses of 1.8, 4.3, 6.1, 8.1 and 10.8 mg, melted with a constant *Hr* of 2 K min^{-1}, were made the object of the mass effect, '*m*', study. An empty hermetically sealed pan was used as reference. The cell was calibrated with an indium standard sample with the same type of hermetically sealed Al pan.

Samples were first quench – cooled to 233–243 K, then allowed to equilibrate at 253 K for 5 min, prior to the melting run. With the liquid nitrogen, 'manual' cooling can, only heating portions are reliable in terms of the temperature program linearity, thus not allowing for a freezing study. Each run consisted of at least two cooling – heating cycles, with differences in successive melting thermal effects not exceeding 2%. Meanwhile, differences between per gram thermal effects (heats of fusion) did not exceed 5% in both '*m*' and '*Hr*' run sets. Sizable differences between the nominal ice melting point (273.15 K) and the onset melting temperatures were observed within both sets of experiments, and were clearly more pronounced in '*m*' runs: they are due both to the thickness of hermetic pans and to the thermal resistances at (a) – the constantan disk/outer pan interface and (b) – inner pan/ice interface. While thermal conduction across interface (a) may be considerably improved by means of thermal lubricants such as high viscosity silicone oil [11] (not used within the present study), interface (b) is probably the main source of lags and shape effects within both heating rate and mass runs. The expected increasing trend of melting temperatures with the increase of heating rate and sample mass is followed.

Prior to the actual fitting, raw data were processed by means of Peakfit 4.0 (Jandel Scientific) software. As the instrument output allows for both temperature plots (*T*) and time plots (*t*), the two alternatives were investigated for all melting endotherms. The first step in data processing consisted of the selection of the X–axis range (i. e. the one within which the recorded signal exhibits significant values) that should be broad enough to afford precise baseline determination. For temperature scaled plots this was 270–290 K; for time scaled plots a time interval of 5 min ('*Hr*' runs) and 7 min ('*m*' runs), equally distributed on both sides of the peak minimum, was found sufficient. As we are mainly concerned with peak shape, aligning of the time-scaled endotherms was preferred to the shifted version of the plot, that we consider characteristic and more appropriate to temperature-scaled endotherms. Further processing involved digital filtering, with a final data count of 1024 points, followed by automated smoothing. Then DuPont DSC 'downward' endotherms were converted by means of the appropriate calculation ($Y_{calc} = -Y_{obs}$) to 'upward' peaks that are suitable for further Peakfit analysis. (For time – scale endotherms an X-axis shift was necessary, so that all peaks start at zero time; this resulted in the positioning of the peak maximum at 2.5 min for '*Hr*' and at 3.5 min for '*m*' experiments.) The next step in data processing involved automatic baseline determination and subtraction. This improves the stability of the fitting process and the fit statistics. The 'Progressive Linear' built-in PeakFit routine was preferred to an imported empty-empty run baseline that could result in the increase of experimental scatter. This automatic fit procedure is suitable for those data sets where it is known that a clear baseline exists at each end of the active data, and consists in progressively fitting a linear model to increasingly more data points, until the goodness of fit deteriorates. As the procedure works in both ascending and descending directions, this choice seems close to the ideal one, i. e. a baseline that is determined by the weighted average between solid and liquid heat capacities. The final step was area normalization resulting in 'normalized heat flows' with reciprocal temperature (*T*-plots) and reciprocal time (*t*-plots) dimensions and peaks of unit area. The obtained data were saved and utilized as 'observed' peaks in the fitting process.

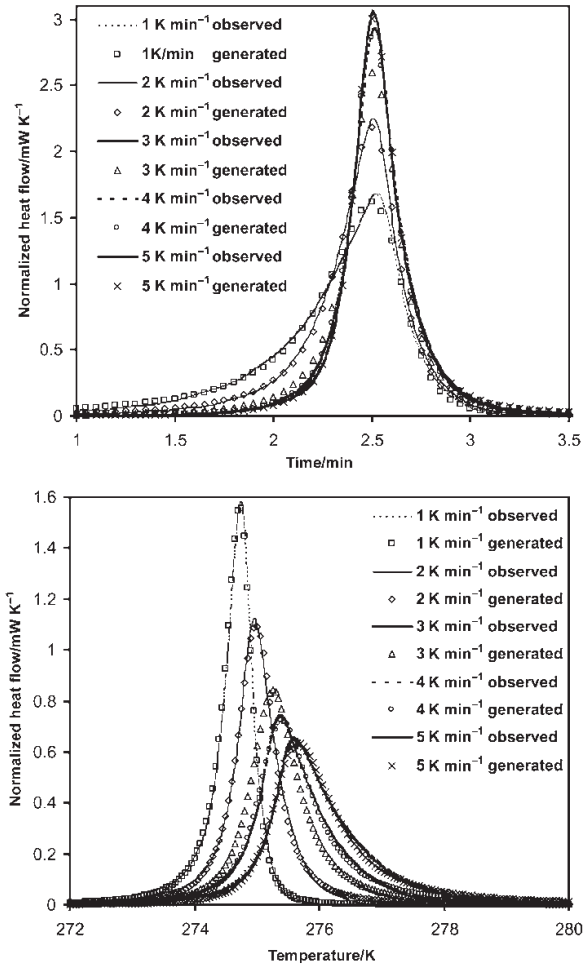

Fig. 1 Pearson IV fits of normalized endotherms obtained at the melting of a 0.3 mg ice sample with various heating rates: *T*=temperature scale and *t*=time scale

Various built-in Peakfit functions were tried for the actual fitting of the above data, the most relevant to this study being summarized in the Appendix. Fitting options included no baseline, no additional smoothing, a 0.5% tolerance in amplitude, variable width and refined shape. A high robust minimization criterion (Pearson 7 limit error) with 1% maximum variation of all parameters was imposed for all fits. Reports were saved and exported in Excel resulting in data sources for 'observed' and 'generated' peaks, as well as for parameters plots. For illustration purposes the time and temperature ranges were further narrowed in all subsequent figures, although data is available over the entire fitting domain.

Results and discussion

Variable heating rate runs

A water sample of 0.3 mg was selected, after preliminary tests, as suitable for the investigation of the heating rate effect. It offered a fairly good signal-to-noise ratio for the lowest heating rate of 1 K min^{-1}; meanwhile, this sample proved to be small enough to consider that 'overload' mass effects are absent. Most of the built-in Peakfit functions were tested: by far the best fitting function proved to be Pearson IV, Eq. (6) in the appendix, within both temperature and time scale plots. This is the function represented in Fig. 1 as 'generated' together with the 'observed' normalized peaks. Experimental (observed) peaks exhibit two significant features:

The first one is their broadness, which is important on both sides of the peak maximum and follows the normal increasing trend with increasing heating rate. This wing-shaped broadening apparently justifies the use of spectral functions such as Lorentz and Voigt as fitting models.

The second one is asymmetry, which presents an interesting behavior: in *T*-plots it shifts from the 'fronted' type at 1 K min^{-1} to a manifest 'tailed' type at 5 K min^{-1}, with an almost symmetrical peak at 2 K min^{-1}; the exactly reversed trend is manifested in *t*-plots. Asymmetry explains the failure of the Lorentz and Voigt functions to satisfactorily represent melting over the whole range of heating rates and justifies the use of chromatographic functions, such as the exponentially modified Gaussian (EMG). However, asymmetric functions of this type fail on the side opposite to the main tailed or fronted wing thus leaving the 5 – parameter Pearson IV (amplitude) as the best choice.

As reported in TMDSC, where hermetic pans were proved responsible for lower precision [12] and for the more pronounced frequency effect and temperature dependence of the heat capacity calibration [9], thermal transfer across the thick walls of these

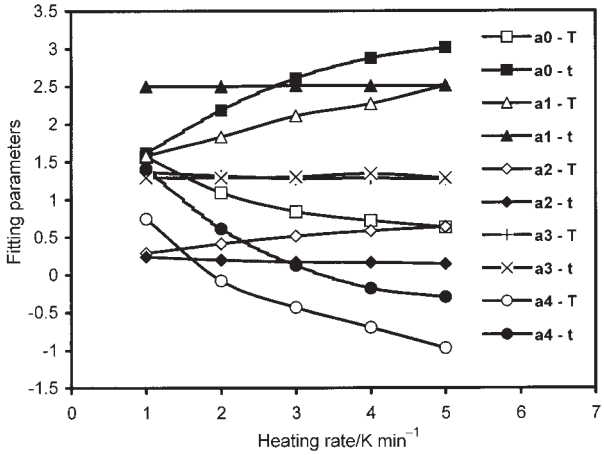

Fig. 2 Variation of Pearson IV fitting parameters with the heating rate, corresponding to: *T*=temperature scale, *t*=time scale plotted peaks of Fig. 1

pans, as well as across their outer and inner interfaces, is probably the main cause of the above-mentioned shape effects. The interplay between the sample thermocouple reading and the real temperature, thus the actual status of the sample inside the hermetic pan, yields an almost symmetric melting endotherm for a heating rate around 2 K min^{-1} in *T*-plots. As discussed later, this reversal occurs between 3 and 4 K min^{-1} for *t*-plots, an indication that some failure in linearity of the heating program may be suspected.

The variation of Pearson IV fitting parameters, presented in Fig. 2 for both *T* and *t* plots, illustrates the above ideas. That of the amplitude parameter, a_0, is evidently non-linear: as apparent in Fig. 1, it decreases with *Hr* (normalized peaks broaden) for *T*-plots, and increases with *Hr* (normalized peaks narrow) for *t*-plots. The width, a_2, follows the normal, opposite trend, with the notable difference that its variation with

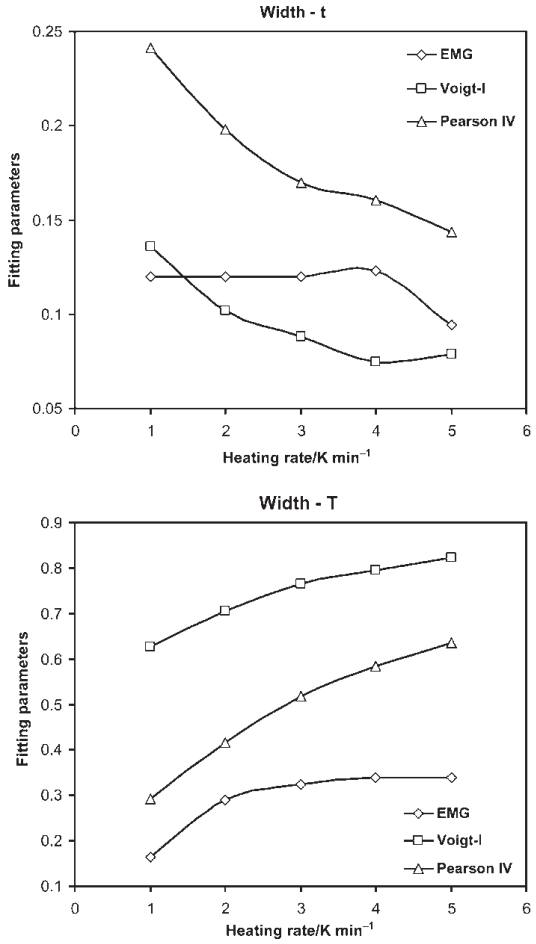

Fig. 3 Width parameter variation with the heating rate for EMG, Voigt and Pearson IV fitting functions, corresponding to: *T*=temperature scale, *t*=time scale plotted normalized endotherms

Hr is fairly close to linear. The center parameter, a_1, (down-shifted with 273.15) linearly increases for *T*-plots, while maintaining the arbitrary chosen (time-scale data processing) value of 2.5 min for *t*-plots. The behavior of the two shape parameters embodied in Pearson IV function is very interesting: The first one, a_3, is almost constant and positioned around the same value, 1.3, for both *T* and *t*-plots. As no restriction was imposed on the fit (no locked parameters) this suggests that the investigated endotherms are represented by a simpler, 4-parameter Pearson IV function, which is intermediate between the Peakfit built-in versions, a_3=1 and a_3=2, offered for chromatographic use. Indeed, fitting both types of peaks with the a_3 parameter locked at

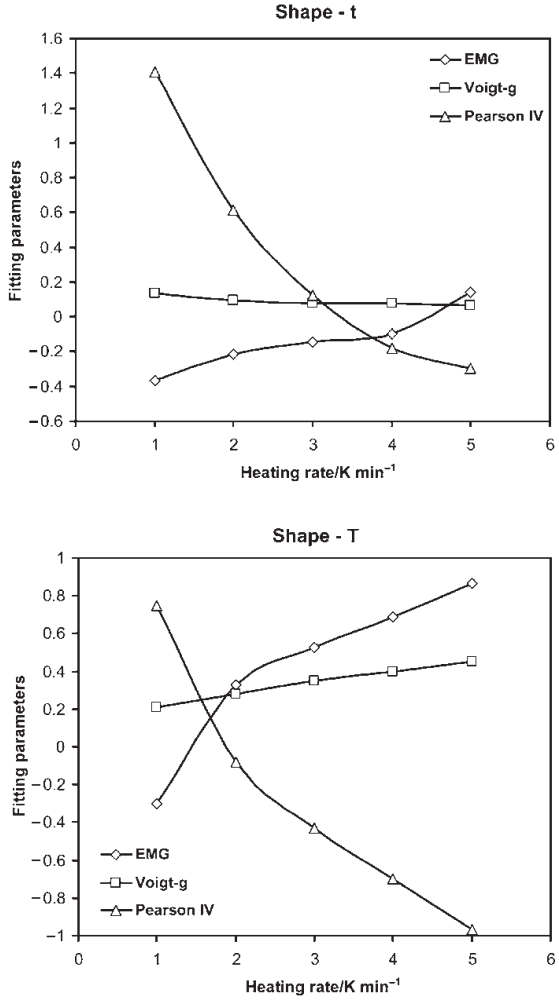

Fig. 4 Shape parameter variation with the heating rate for EMG, Voigt and Pearson IV fitting functions, corresponding to: *T*=temperature scale, *t*=time scale plotted normalized endotherms

1.3 resulted in no significant modifications of the other parameters values, with the same very good standard errors (SE<0.02) and correlation coefficients (r^2>0.995). Asymmetry is thus embodied in the a_4 parameter, which is positive for fronted and negative for tailed peaks. In contrast with all other parameters, a_4 follows the same decreasing trend for both types of plots, with the steepest variation between 1 and 2 K min^{-1}. For T-plots the sign change occurs within this Hr range while its variation for the remaining Hr values is close to linear. For t-plots the whole trend is non-linear and parameter a_4 changes its sign between 3 and 4 K min^{-1}.

One may conclude, within the given experimental setup described in the previous section, that the most important instrumental contribution at the variation of heating rate

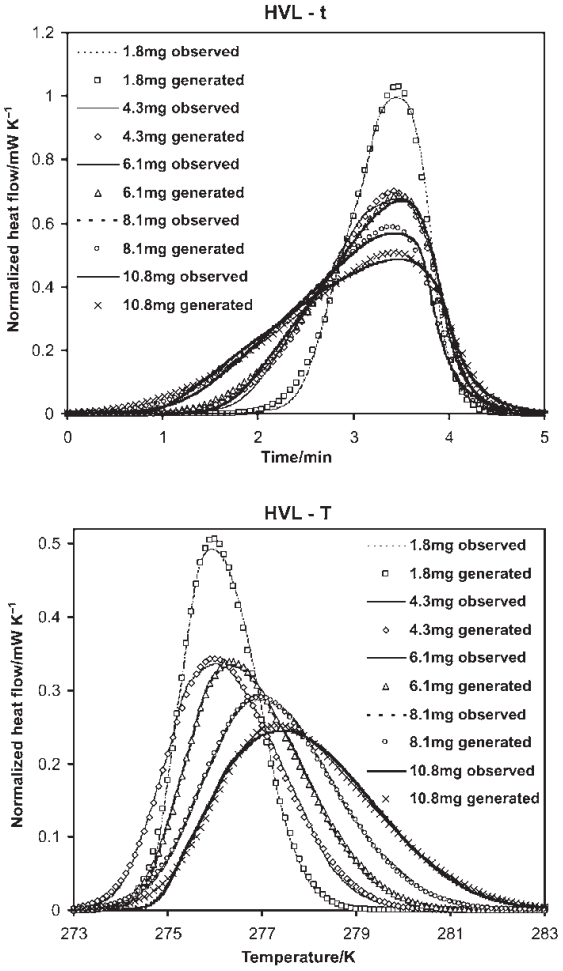

Fig. 5 HVL fits of normalized endotherms obtained at the melting of a varying mass ice samples with 2 K min^{-1} heating rate: T=temperature scale and t=time scale plots

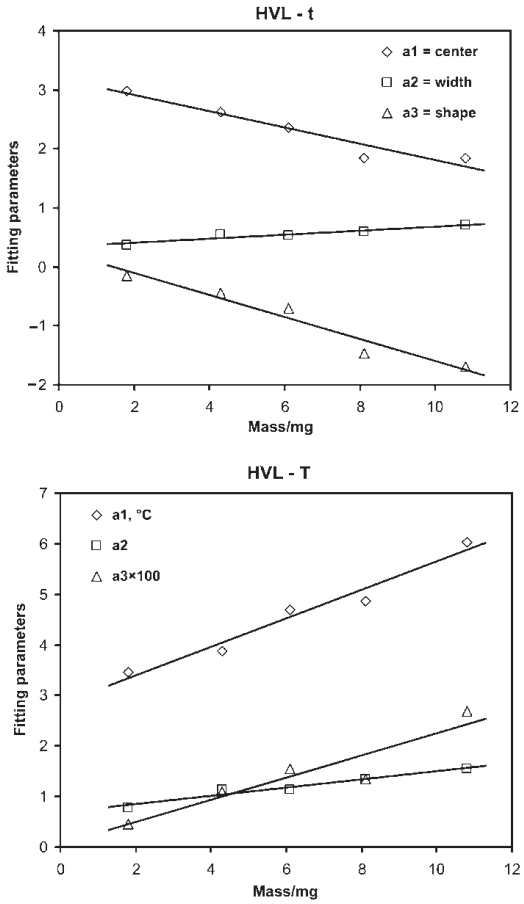

Fig. 6 Mass variation of HVL fitting parameters pertaining to the normalized endotherms presented in Fig. 5: *T*=temperature scale and *t*=time scale peaks

is embodied in the key shape parameter, a_4, of the Pearson IV function. In *T*-scale plotted curves, common to most DTA and DSC reported experiments, signal broadening and shift of peak temperature with increasing *Hr* is well known. A change in shape, as the one described here, is most important for at least two reasons: 1) It offers essential information for the separation of two overlapping peaks and for any attempt to separate the 'pure' sample signal from the instrumental one. 2) It may affect non-isothermal kinetic studies, in which working at several heating rates is nowadays mandatory, in the sense that an instrumental feature could be taken for the 'real thing'.

Comparison between Pearson IV and other fitting functions is instructive. For reasons of space this was limited to a spectroscopic alternative (Voigt, which may give good results for symmetrical peaks) and a chromatographic one (EMG, which is suitable for asymmetrical peaks). The width and shape (distortion) parameters of all three functions are presented in Figs 3–4. One should emphasize that the overall fit quality of Voigt and

EMG is considerably lower than that of Pearson IV even in most favorable cases. As the Voigt function is the convolution between a 'true' Lorentzian-shaped signal and a Gaussian instrumental 'smearing', the former is held responsible for 'width', while the later accounts for 'shape'.

The width parameters all follow a monotonous trend for *T*-plots, illustrated in Fig. 3. This is no longer valid for *t*-plots, where the monotonous variation of the fitting parameters breaks down for Voigt and EMG. The main reason is not a possible deviation from linearity of the heating program, but rather the fitting failure of these two functions: with no constraints imposed, the search for the best fit may lead to reversals in the values of width parameters.

The variation of the shape parameters, presented in Fig. 4, is even more instructive. As expected, the symmetrical Voigt function is unable to predict the fronted-to-tailed transition and the quasi-linear variation of the Voigt shape parameter is misleading. On the contrary, the asymmetrical EMG predicts this transition almost correctly (although with a shift to 4–5 K min^{-1} in the case of *t*-plots) albeit the fit quality is well below that of the Pearson IV. We thus came to an evident conclusion: asymmetrical peaks (such as the vast majority of DTA and DSC thermal effects), even if their asymmetry is not obvious at first sight, should not be described by means of spectroscopic peak functions.

Variable mass runs

The straightforward solution to minimize instrumental effects such as the above-described 'wings' is to increase the sample mass. Figure 5 presents the data obtained (and processed as described in the experimental section) in 5 runs with different sample masses and a common heating rate of 2 K min^{-1}. The observed peaks display broadening and asymmetry, which is again reversed, exactly as in the *Hr* case: peaks are tailed in *T*-plots and fronted in *t*-plots. However, the broadening trend is now conserved in both types of plots: broadness increases with sample mass. While this behavior is trivial in thermal analysis, fitting normalized peaks with the Haarhoff–Van der Linde function (HVL, Eq. (5) in appendix) is not.

This function was derived [13] to take into account axial diffusion and dispersion effects in gas chromatographic (GC) systems with column overloading and assumed adsorption equilibrium. The model predicts that column overloading with Langmuir adsorption yields tailed chromatographic peaks, while anti-Langmuir adsorption results in fronted ones. (HVL is the only non-empirical Peakfit function capable of modeling fronted peaks.) One may easily notice that the time–scale (which is also the chromatographic scale) representation of DSC endotherms of Fig. 5 is fronted. Is that coincidental? The answer is, most probably, no.

We are clearly dealing with an overload effect, manifested in the propagation of heat within the sample and thus with the propagation of the melting process itself. As thermal transfer is much better across the contact zone between the solid sample and Al pan, initial partial melting with the formation of an interface liquid layer with dif-

ferent thermal properties is perfectly conceivable. The remainder of the process would be melting of an ice kernel surrounded by liquid water.

With the important differences of size and non-isothermal regime, the situation is quite similar with the 'water-on-the-rocks' experiments of Galwey *et al.* [10], in the interpretation of which it was assumed that 'melting rate control is by heat transfer'. Size is an essential factor here: we do not expect the occurrence of such phenomena in the case of 'small' samples, such as the one utilized in the evaluation of heating rate influence.

Other functions able to describe peak asymmetry were also tried. In some cases, such as Beta (amplitude) and Pearson IV, *SE* and r^2 values were close to (and in some instances better than) the HVL ones ($SE<0.3$, $r^2>0.992$), but with large uncertainties in the width and shape fitting parameters. This is not the case with HVL, which clearly offers the best description of the presented variable mass data. As illustrated in Fig. 6, the center, width and shape parameters follow a definite linear trend (extremely useful for calibration purposes) in both *T* and *t*-plots, with a normal scatter due to experimental errors. (Figure 5 also reflects a too close resemblance between peaks corresponding to 6.1 and 8.1 mg samples.) Until further checking, we may safely conclude that overload in DSC ice melting endotherms is best described by the HVL function which models the GC overload effects. To our best knowledge, such an analogy is entirely novel.

Conclusions

This study may be regarded as a first attempt, and at the same time a suggestion, to interpret thermal (DSC) data by means of advanced tools of spectroscopy and chromatography. Melting of ice was chosen as a test process because it yields well-defined, yet complex endotherms. The influence of two typical thermoanalytical factors, heating rate and sample mass, was investigated.

Within the available experimental setup (DuPont 1090 DSC with hermetically sealed aluminum pans and stainless steel cooling can under liquid nitrogen) heating rate effects are best reflected by the Pearson IV function. This may be considered as representing the instrumental profile, determined mainly by thermal transfer across the interfaces and the thick walls of hermetic pans. An important change in shape takes place, within the investigated heating rate range, for normalized endotherms plotted in both temperature and time scale: peaks turn from fronted to tailed. This may be a source of errors (artifacts) in non-isothermal kinetics whenever low sample masses and/or low thermal signals are studied.

Mass overload effects are properly described by the GC function Haarhoff–Van der Linde (HVL). As thermal transfer within the sample and across the liquid interface formed by partial melting plays the key role in this case, the analogy with a chromatographic model derived to account for axial dispersion and diffusion in an overloaded column seems justified. The HVL fitting capabilities are most probably not accidental and the analogy between gas flow and thermal flow deserves further investigation.

The thick walls of hermetic sealed pans and their inner and outer interfaces play an important role in the shape of the observed endotherms. Supported by the suffi-

ciently low vapor pressure of ice around its melting point, a check with normal pans appears to be the natural extension of the present work. So does the study of other materials, e.g., metals, as well as the investigation of shape affecting factors such as the DSC cell gaseous atmosphere. These will be dealt with in subsequent contributions.

As clearly stated in its title, this article is an attempt towards the systematic determination of DSC instrumental profiles. Although making use of functions pertaining to spectroscopy and chromatography signal processing seems promising, much more experimental data and case studies are needed to establish a reliable correlation between thermal parameters of the calorimeter and curve fitting parameters, i.e. to ascribe a clear physical significance to the latter.

* * *

This work was supported by MEC under Grant Nr. 6124 / 2000.

References

1 S. Sauerbrun, B. Crowe and M. Reading, American Laboratory, 8 (1992) 44.
2 M. Reading, D. Elliot and V. L. Hill, J. Thermal Anal., 40 (1993) 949.
3 B. Wunderlich, Y. Jin, and A. Boller, Thermochim. Acta, 238 (1994) 277.
4 B. Wunderlich, A. Boller, I. Okazaki and S. Kreitmeier, Thermochim. Acta, 282/283 (1996) 143.
5 M. Brun, A. Lallemand, J. F. Quinson and C. Eyraud, Thermochim. Acta, 21 (1977) 59.
6 J. Desbrierres, M. Rinando and M. Brun, J. Chim. Phys., 78 (1981) 187.
7 L. Zeeman and G. Tkacik, J. Membrane Sci., 32 (1987) 329.
8 F. P. Cuperus, D. Bargeman and C. A. Smolders, J. Membrane Sci., 66 (1992) 45.
9 S. A. Knopp and S. L. Nail, J. Therm. Anal. Cal., 60 (2000) 319.
10 A. K. Galwey, D. B. Sheen and J. N. Sherwood, Thermochim. Acta, 375 (2001) 161.
11 J. H. Flynn, Thermochim. Acta, 217 (1993) 133.
12 M. Varma-Nair and B. Wunderlich, J. Thermal Anal., 46 (1996) 879.
13 P. H. Haarhoff and H. J. Van der Linde, Anal. Chem., 38 (1966) 573.

Appendix

The main functions utilized in this work are presented below:

'Spectral' (symmetrical) functions

Gaussian (area):

$$y=\frac{a_0}{a_2\sqrt{2\pi}}\exp\left[-\frac{1}{2}\left(\frac{x-a_1}{a_2}\right)^2\right] \quad (1)$$

a_0=area, a_1=center, a_2=width (>0);

Lorentzian (area):

$$y=\frac{a_0}{\pi a_2\left[1+\left(\frac{x-a_1}{a_2}\right)^2\right]} \tag{2}$$

a_0=area, a_1=center, a_2=width (>0);

Voigt (area):

$$y=\frac{a_0}{a_2\sqrt{\pi}}\int_{-\infty}^{\infty}\frac{\exp(-t^2)}{a_3^2+\left(\frac{x-a_1}{a_2}-t\right)^2}\mathrm{d}t \tag{3}$$

a_0=area, a_1=center, a_2=width (>0), a_3=shape (≥0)

'Chromatographic' (asymmetrical) functions

Exponentially modified Gaussian (EMG):

$$y=\frac{a_0}{2a_3}\exp\left(\frac{a_2^3}{2a_3^2}+\frac{a_1-x}{a_3}\right)\left[erf\left(\frac{x-a_1}{a_2\sqrt{\pi}}-\frac{a_2}{a_3\sqrt{\pi}}\right)+\frac{a_3}{|a_3|}\right] \tag{4}$$

a_0=area, a_1=center, a_2=width (>0), a_3=distortion (shape) (≠0)

Haarhoff–Van der Linde (HVL):

$$y=\frac{a_0\exp\left(-\frac{1}{2}\frac{(x-a_1)^2}{a_3^2+a_2^2}\right)\left[1+erf\left(\frac{a_3(x-a_1)}{a_2\sqrt{2}\sqrt{a_3^2+a_2^2}}\right)\right]}{\sqrt{2\pi}\sqrt{a_3^2+a_2^2}} \tag{5}$$

a_0=area, a_1=center, a_2=width (>0), a_3=distortion (shape) (≠0)

Pearson IV (amplitude):

$$y=\frac{a_0\left[1+\frac{\left(x-\frac{a_2a_4}{2a_3}-a_1\right)^2}{a_2^2}\right]^{-a_3}\exp\left[-a_4\left(\tan^{-1}\left(\frac{x-\frac{a_2a_4}{2a_3}-a_1}{a_2}\right)+\tan^{-1}\left(\frac{a_4}{2a_3}\right)\right)\right]}{\left(1+\frac{a_4^2}{4a_3^2}\right)^{-a_3}} \tag{6}$$

a_0=amplitude, a_1=center, a_2=width (>0), a_3=shape 1 (≠0), a_4=shape 2.